Journal of Sound and Vibration (2000) **230**(5), 1069–1101
doi:10.1006/jsvi.1999.2663, available online at http://www.idealibrary.com on IDEAL®

CORRELATIONS BETWEEN DYNAMIC STRAIN AND VELOCITY IN RANDOMLY EXCITED PLATES AND CYLINDRICAL SHELLS WITH CLAMPED BOUNDARIES

D. G. KARCZUB AND M. P. NORTON

Department of Mechanical and Materials Engineering, Centre for Acoustics, Dynamics and Vibration, The University of Western Australia, Nedlands, Western Australia, 6907*, Australia*

(*Received* 5 *February* 1998, *and in final form* 8 *September* 1999)

Relationships for the correlation of dynamic strain and velocity in randomly vibrating plates and cylindrical shells are derived. These relationships are of interest for practical predictions of maximum dynamic strain from simple vibrational velocity measurements obtained using accelerometers, and are based on (1) farfield relationships between the propagating wave components of dynamic strain and velocity, (2) factors for the effects of evanescent waves, and (3) the correlation of dynamic strain and velocity spatial maxima in narrow frequency bands. Spatial distributions of dynamic bending strain and velocity are also presented depicting the propagating wave component of the response, correlations between dynamic strain and velocity, evanescent wave effects and dynamic stress concentration at clamped boundaries. Experimental results are presented supporting the use of derived relationships for the measurement of maximum dynamic strain. The derived relationships apply equally to narrowband and broadband-excited systems by avoiding the need to satisfy diffuse wave conditions.

1. INTRODUCTION

Correlations between dynamic strain and velocity are of interest in the development of practical methods for the measurement of maximum dynamic stress and strain in randomly vibrating structures. In a related paper [1], previously developed relationships [2, 3] for single-mode flexural vibration of thin beams were formalized and extended to multi-modal vibration at and above the first natural frequency. This involved the use of factors for the effects of evanescent waves on the fundamental farfield relationship between dynamic strain and velocity; the correlation of dynamic strain and velocity spatial maxima in narrow frequency bands; and the summation of predicted narrow-band spatial maximum values to obtain conservative overall multi-modal predictions of dynamic strain. The predicted spatial maximum values in narrow frequency bands f_i are given by

$$\langle \xi^2_{max,pred}(f_i)\rangle = K'(f_i)\frac{K_{shape}}{c_L}\langle v^2_{max}(f_i)\rangle = \frac{K(f_i)}{c_L}\langle v^2_{max}(f_i)\rangle, \tag{1}$$

0022-460X/00/101069 + 33 $35.00/0

and the overall multi-modal prediction of dynamic strain is given by

$$\langle \xi^2_{max,pred} \rangle \leqslant \sum_{i=1}^{\infty} \langle \xi^2_{max,pred}(f_i) \rangle = \sum_{i=1}^{\infty} \frac{K(f_i)}{c_L} \langle v^2_{max}(f_i) \rangle, \tag{2}$$

where ξ is dynamic strain, v is velocity, K' is a factor for evanescent wave effects on the farfield spatial maxima of dynamic strain and velocity, $\langle\rangle$ represents the time average, K_{shape} is the non-dimensional shape factor, and K is the non-dimensional correlation ratio between the spatial maxima of dynamic strain and velocity.

In the present paper, the same approach is used to derive narrowband relationships between dynamic strain and velocity for random vibration of transversely excited plates and cylindrical shells similar to equation (1) that can be used with equation (2) to obtain conservative overall predictions of spatial maximum dynamic strain. The derived relationships have the same generic form as those defined for beam vibration providing the basis for a consistent theoretical and experimental approach to the prediction of dynamic stress and strain in beams, plates and cylindrical shells. In the development followed here, the sum of dynamic bending strains in orthogonal directions is taken as the upper-bound value of dynamic strain in farfield regions. This is assumed to be justified on the basis that (1) shear strain is equal to zero at locations of maximum farfield dynamic bending strain, and (2) the results are expected to be sufficiently conservative to account for any increase in maximum overall dynamic strain due to in-plane shear strain. The accuracy of this assertion is tested by way of calculation for the vibration of clamped cylindrical shells using the maximum principal strain to represent the complex stress state presented by two in-plane orthogonal components of bending strain and one component of in-plane shear strain.

Relationships for the prediction of maximum dynamic stress/strain in plates and cylindrical shells from vibrational velocity data have also been investigated by Hunt [2], Ungar [3], Stearn [4, 5], and Norton and Fahy [6]. Hunt and Ungar considered the single-mode vibration of beams, simply supported plates and clamped circular plates. Stearn considered the farfield broad band vibration of plates and provided factors relating spatially averaged farfield data to maximum levels of dynamic stress at clamped boundaries. Relationships between dynamic stress and velocity derived by Stearn are based on the assumption of a diffuse wave field and are therefore limited to broadband excited structures in which 10 or more modes are excited with similar amplitudes of vibration. In the work by Stearn only one component of dynamic bending stress, which is averaged over all directions, is considered, and dynamic shear strain is neglected. Norton and Fahy apply the relationships given by Stearn to an experimental analysis of broadband correlations between dynamic strain and velocity in constrained and unconstrained cylindrical shells. Their experimental results support the use of correlations between dynamic strain and velocity, but the interpretation of results is limited by a lack of supporting work in the literature on the dynamic stress/strain response of cylindrical shells and theoretical correlations between dynamic strain and velocity.

The work contained in the current paper also serves as a study on the effects of evanescent waves and the direction of wave propagation on dynamic strain. Increased dynamic strain at a boundary or discontinuity is referred to as dynamic stress/strain concentration and was first studied by Ungar [7] for semi-infinite plates with a reinforcing beam discontinuity. The only other published works on dynamic stress concentration in plates are studies by Stearn [4, 5] on dynamic stress concentration at clamped boundaries and step changes in thickness of semi-infinite plates. These latter studies were based on the assumption of a diffuse wave field for statistical energy analysis applications. The only published data showing dynamic stress concentration in cylindrical shells is contained in a paper by Forsberg [8], an internal report by Steele [9] referenced by Forsberg, and some experimental broadband results reported by Norton and Fahy [6].

Dynamic stress concentration effects are demonstrated explicitly in this paper by separately plotting the spatial distributions of the propagating and evanescent wave components of the response, in addition to the spatial distribution of total dynamic strain. An important consideration identified here for cylindrical shell vibration is the effect of additional pairs of evanescent waves with much smaller wavelength (and hence increased wavenumber) than the propagating wave component of the response. These additional evanescent waves result in short regions of increased dynamic strain which are difficult to measure using strain gauges.

2. FLEXURAL VIBRATION OF THIN RECTANGULAR PLATES

The aims of this section are to investigate the extension of principles and relationships established for the analysis of beam flexural vibration to the analysis of transversely excited thin rectangular plates, and to analyze dynamic strain concentration effects in rectangular plates. The main factor influencing the response of rectangular plates is identified as the direction of wave propagation.

2.1 TRAVELLING WAVE SOLUTIONS

The approximate travelling wave solution derived by Karczub [10] for fully constrained plates is used here to obtain analytical solutions for the analysis of dynamic strain and velocity in clamped rectangular plates. The approximate solution simplifies to the exact *Levy*-type solution for two opposite sides simply supported. The approximate solution has been used here as the clamped plate system best demonstrates the effects of interest here and an exact solution does not exist.

2.1.1. *The approximate travelling wave solution*

The approximate travelling wave solution for a constrained rectangular plate is given by

$$\boldsymbol{w}(x, y, k_x, k_y) = \boldsymbol{w}_x(x, k_x)\boldsymbol{w}_y(y, k_y), \tag{3}$$

where

$$\boldsymbol{w}_x(x, k_x) = \mathbf{A}_x e^{-ik_x x} + \mathbf{B}_x e^{ik_x x} + \mathbf{C}_x e^{-x\sqrt{k_x^2 + 2k_y^2}} + \mathbf{D}_x e^{x\sqrt{k_x^2 + 2k_y^2}} \tag{4}$$

and

$$\boldsymbol{w}_y(y, k_y) = \mathbf{A}_y e^{-ik_y y} + \mathbf{B}_y e^{ik_y y} + \mathbf{C}_y e^{-y\sqrt{2k_x^2 + k_y^2}} + \mathbf{D}_y e^{y\sqrt{2k_x^2 + k_y^2}}. \tag{5}$$

In equation (3), $\boldsymbol{w}$ is the complex displacement at position (x, y); $k_x = k_B \cos\theta$ is the x-component of the bending wavenumber k_B; $k_y = k_B \sin\theta$ is the y-component of k_B; θ is the direction of wave propagation; $k_B^4 = (k_x^2 + k_y^2)^2 = \rho h\omega^2/D$; h is the plate thickness; $\omega = 2\pi f$ is the angular frequency; $D = Eh^3/12(1 - \mu^2)$; and μ is the Poisson ratio.

Expansion of equation (3) after substituting equations (4) and (5) reveals that only those terms with evanescent wave components in both directions are incorrect when compared with the complete travelling wave solution. As the influence of these terms is restricted to the corners of a constrained rectangular plate where the dynamic bending strain and velocity response tend to zero, the approximate travelling wave solution defined by equations (3)–(5) is expected to be reasonably accurate for plates with combinations of clamped and/or simply supported boundary conditions. For the case of any two opposite sides simply supported, the problem of incompatible wavenumbers in the x and y directions does not arise and the solution is exact. Natural frequencies calculated for clamped rectangular plates using the approximate travelling wave solution compare well with published values (refer Appendix A).

2.1.2. *Travelling wave solutions for dynamic bending strain and velocity*

The dynamic bending strains at the plate surface in the x and y directions for flexural vibration of a plate, expressed in terms of the approximate travelling wave solution, are given by

$$\xi_x(x, y, k_x, k_y) = z_m \frac{\partial^2 \boldsymbol{w}}{\partial x^2} = z_m \frac{\mathrm{d}^2 \boldsymbol{w}_x(x, k_x)}{\mathrm{d}x^2} \boldsymbol{w}_y(y, k_y) \tag{6}$$

and

$$\xi_y(x, y, k_x, k_y) = z_m \frac{\partial^2 \boldsymbol{w}}{\partial y^2} = z_m \boldsymbol{w}_x(x, k_x) \frac{\mathrm{d}^2 \boldsymbol{w}_y(y, k_y)}{\mathrm{d}y^2}, \tag{7}$$

and the transverse velocity from equation (3) is simply

$$\boldsymbol{v}(x, y, k_x, k_y) = i\omega \boldsymbol{w}_x(x, k_x) \boldsymbol{w}_y(y, k_y), \tag{8}$$

where z_m is the distance of the outermost fibre from the centroidal axis. If farfield conditions are assumed and evanescent waves are neglected, the dynamic bending

strains are given by

$$\xi_{x,FF}(x, y, k_x, k_y) = z_m k_x^2 \boldsymbol{w}_{x,FF}(x, k_x)\boldsymbol{w}_{y,FF}(y, k_y)$$
$$= z_m k_B^2 \cos^2\theta \boldsymbol{w}_{x,FF}(x, k_x)\boldsymbol{w}_{y,FF}(y, k_y) \quad (9)$$

and

$$\xi_{y,FF}(x, y, k_x, k_y) = z_m k_y^2 \boldsymbol{w}_{x,FF}(x, k_x)\boldsymbol{w}_{y,FF}(y, k_y)$$
$$= z_m k_B^2 \sin^2\theta \boldsymbol{w}_{x,FF}(x, k_x)\boldsymbol{w}_{y,FF}(y, k_y), \quad (10)$$

whilst the velocity is given by

$$\boldsymbol{v}_{FF}(x, y, k_x, k_y) = \mathrm{i}\omega \boldsymbol{w}_{x,FF}(x, k_x)\boldsymbol{w}_{y,FF}(y, k_y). \quad (11)$$

The displacement components $\boldsymbol{w}_{x,FF}$ and $\boldsymbol{w}_{y,FF}$ are given by equations (4) and (5), respectively, but with $\boldsymbol{C}_x$, $\boldsymbol{D}_x$, $\boldsymbol{C}_y$ and $\boldsymbol{D}_y$ all set to zero leaving only the propagating wave components.

2.2. FARFIELD RELATIONSHIPS

Farfield relationships between the propagating wave components of dynamic strain and velocity are derived as follows. These relationships provide the theoretical basis for correlating the spatial maxima of dynamic bending strain and velocity in narrow-frequency bands for the prediction of maximum dynamic bending strain.

2.2.1. *Relationships for the components of dynamic bending strain*

The dynamic bending strains in equations (9) and (10) are related to velocity in the farfield by

$$\frac{\xi_{x,FF}(x, y, k_x, k_y)}{\boldsymbol{v}_{FF}(x, y, k_x, k_y)} = \frac{z_m k_B^2 \cos^2\theta}{\mathrm{i}\omega} = \frac{-\mathrm{i}K_{shape}}{c_L}\cos^2\theta \quad (12)$$

and

$$\frac{\xi_{y,FF}(x, y, k_x, k_y)}{\boldsymbol{v}_{FF}(x, y, k_x, k_y)} = \frac{z_m k_B^2 \sin^2\theta}{\mathrm{i}\omega} = \frac{-\mathrm{i}K_{shape}}{c_L}\sin^2\theta, \quad (13)$$

where $K_{shape} = z_m\sqrt{A/I}$ is the non-dimensional geometric shape factor (which equals $\sqrt{3}$, independent of plate thickness), A is the cross-sectional area, I is the area moment of inertia, and c_L is the longitudinal wave speed for a plate given by $c_L = \sqrt{E/\rho(1-\mu^2)}$.

These are the same relationships as for flexural vibration of a beam except that for plate vibration (1) the farfield correlation ratio between a component

of dynamic bending strain and velocity is a function of the direction of wave propagation and (2) there are two bending strain components, each with a different farfield correlation ratio. Since the dominant direction of wave propagation varies from one frequency to the next and is generally not known from vibration measurements, exact predictions of dynamic bending strain from velocity using the above relationships are not possible.

2.2.2. *Relationships based on the sum of dynamic bending strain components*

If the dynamic bending strain component sum $\xi_{x,FF} + \xi_{y,FF}$ is related to velocity (in place of the individual components of dynamic bending strain), the wavenumber independent relationship

$$\frac{\xi_{x,FF}(x, y, k_x, k_y) + \xi_{y,FF}(x, y, k_x, k_y)}{v_{FF}(x, y, k_x, k_y)} = \frac{z_m k_B^2}{\mathrm{i}\omega} = \frac{-\mathrm{i}K_{shape}}{c_L} \tag{14}$$

results. As this relationship is independent of the direction of wave propagation for vibration at frequency f, it can be re-expressed as

$$\frac{\xi_{x,FF}(x, y, f) + \xi_{y,FF}(x, y, f)}{v_{FF}(x, y, f)} = \frac{z_m k_B^2}{\mathrm{i}\omega} = \frac{-\mathrm{i}K_{shape}}{c_L}. \tag{15}$$

This relationship is equivalent to the farfield relationship between dynamic bending strain and velocity for beam flexural vibration. It is independent of plate thickness, frequency and the direction of wave propagation.

Comparing equation (15) with equations (12) and (13), it is seen that the sum of dynamic bending strains in equation (15) provides an upper bound value for the components of dynamic bending strain in farfield regions. The results for cylindrical shell vibration in section 3 indicate that this also represents the upper-bound value of the maximum principal strain taking account of dynamic shear strain in addition to the two components of dynamic bending strain. Equation (15) can be used with equations (1) and (2) for upper-bound predictions of maximum dynamic bending strain in farfield regions.

2.3. MODAL SPATIAL DISTRIBUTIONS

The approximate travelling wave solution presented in section 2.1.1 is used in this section to analyze the modal spatial distributions of dynamic bending strain and velocity in a clamped rectangular plate. The system dimensions are given in Figure 1, and the values of $m, n, f_{m,n}, k_x, k_y$ and θ for each of the first 10 natural frequencies are listed in Table 1.

2.3.1. *Calculation procedures*

The wavenumber component magnitudes k_x and k_y are solved simultaneously from the determinant of the boundary condition matrix for natural frequency (m, n). Once k_x and k_y are known, the complex constants in the x and y directions are

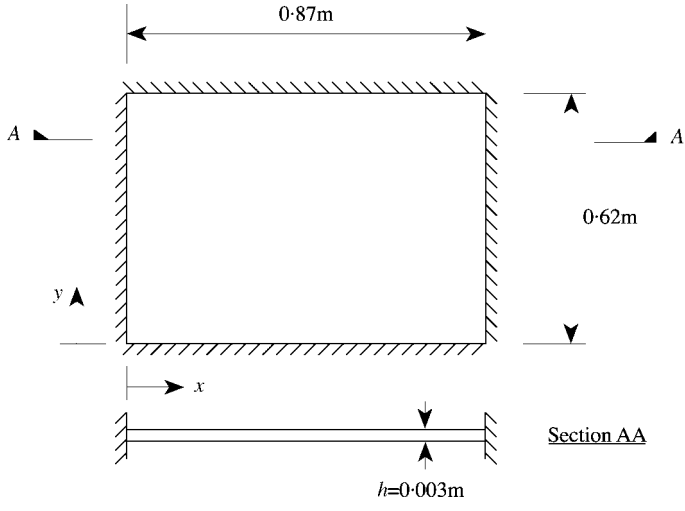

Figure 1. Clamped rectangular plate system.

solved separately using the same procedures as for the vibration of a one-dimensional beam. The modal spatial distributions for dynamic bending strain are then calculated using the expressions

$$\xi_x(x, y, k_x, k_y) = -z_m \boldsymbol{w}_y(y, k_y)(-k_x^2 \mathbf{A}_x e^{-ik_x x} - k_x^2 \mathbf{B}_x e^{ik_x x} + (k_x^2 + 2k_y^2)\mathbf{C}_x e^{-x\sqrt{k_x^2+2k_y^2}} + (k_x^2 + 2k_y^2)\mathbf{D}_x e^{x\sqrt{k_x^2+2k_y^2}}) \quad (16)$$

and

$$\xi_y(x, y, k_x, k_y) = -z_m \boldsymbol{w}_x(x, k_x)(-k_y^2 \mathbf{A}_y e^{-ik_y y} - k_y^2 \mathbf{B}_y e^{ik_y y} + (2k_x^2 + k_y^2)\mathbf{C}_y e^{-y\sqrt{2k_x^2+k_y^2}} + (2k_x^2 + k_y^2)\mathbf{D}_y e^{y\sqrt{2k_x^2+2k_y^2}}), \quad (17)$$

whilst the velocity response is calculated from equation (8). The predicted dynamic strain is calculated from velocity using the farfield relationship

$$\xi_{pred}(x, y, f) = \frac{K_{shape}}{c_L} v(x, y, f) \quad (18)$$

which follows from equation (15), where K_{shape} equals $\sqrt{3}$ and c_L is defined in Section 2.2.1. As the spatial distributions along a line $x = constant$ or $y = constant$ are independent of the response in the normal direction, the two normal directions can be analyzed independently.

2.3.2. *Spatial distributions*

Spatial distributions of dynamic bending strain for the fourth natural frequency of the clamped plate in Figure 1 are plotted in Figure 2. These spatial distributions

are presented as slices parallel to the plate edges, passing through the position of maximum velocity. The spatial distributions in the x direction are for the dynamic bending strain ξ_x and the predicted dynamic strain ξ_{pred} from equation (18); the spatial distributions in the y direction are for the dynamic bending strain ξ_y and the predicted dynamic strain ξ_{pred}. Response levels are normalized to give unit predicted dynamic strain at the position of maximum velocity. The propagating and evanescent wave components of the velocity response are also shown, plotted after scaling according to equation (18) to give "predicted" dynamic strain, for comparison with the spatial distributions of dynamic strain and total velocity.

2.3.3. *Wavenumber effects on farfield dynamic strain levels*

The propagating wave component of dynamic bending strain in the x direction (ξ_x) is proportional to k_x^2, whilst the propagating wave component of dynamic bending strain in the y direction (ξ_y) is proportional to k_y^2 (refer equations (9) and (10)). Since $k_x^2 + k_y^2$ equals k_B^2, a large value of k_x^2 relative to k_B^2 implies a small value of k_y^2, and *vice versa*. As a consequence of these effects, the direction with the larger value of (k_x, k_y) will be the component direction with the highest level of dynamic bending strain. This is demonstrated by the dominance of ξ_x in Figure 2 for $k_x > k_y$ (mode (4, 1)). The values of k_x and k_y, as well as the direction of wave propagation, are listed in Table 1. As their values vary from one mode to the next, the relative magnitudes and the largest component of farfield dynamic bending strain will also vary.

2.3.4. *Dynamic strain concentration*

Dynamic strain concentration is observed at the clamped boundaries of the plate for both ξ_x and ξ_y. Dynamic strain concentration is a result of evanescent wave effects and is a function of both k_x^2 and k_y^2, as seen from equations (16) and (17). The level of dynamic strain concentration is largest for the bending strain component with the smallest propagating wavenumber component magnitude and the lowest level of farfield dynamic bending strain. However, maximum dynamic bending strain occurs in the component direction that has the smallest level of dynamic strain concentration but the largest level of farfield dynamic bending strain. For instance, in Figure 2 for mode (4,1), dynamic strain concentration is largest for ξ_y (the y direction wavenumber component magnitude ($k_y = 6{\cdot}1$) is smaller than in the x direction ($k_x = 12{\cdot}4$)), whilst the dynamic strain ξ_x is much larger in spite of a smaller value of dynamic strain concentration.

It is also useful to note that the travelling wave equation for a component of dynamic bending strain approximates the equation for dynamic strain in a beam as the bending wavenumber component in that direction tends to k_B. Therefore, for shallow angles of wave propagation (θ close to 0 or $\pi/2$), the level of dynamic strain concentration tends to the level of dynamic strain concentration in a beam in the component direction with the largest level of dynamic strain. Inspection of equations (16) and (17) also reveals that the level of dynamic strain concentration in plates is always larger than in beams due to coupling with the normal direction of

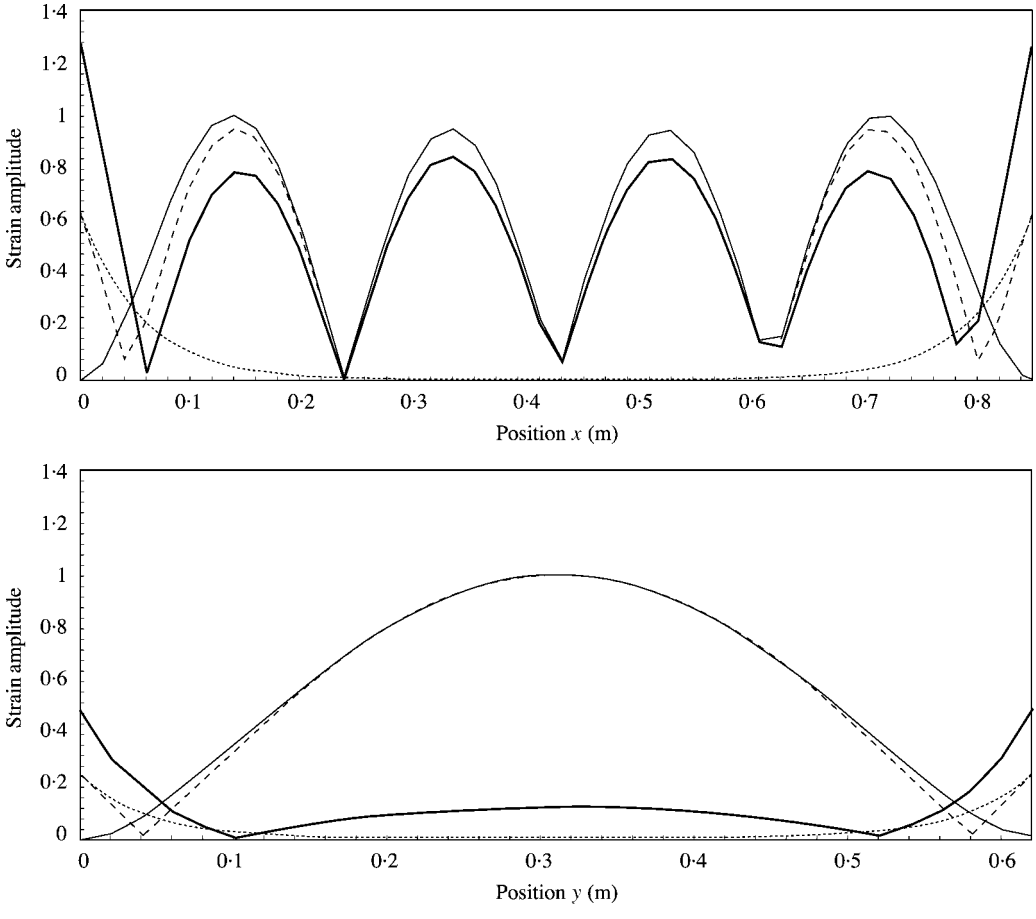

Figure 2. Modal spatial distributions of a clamped plate for mode (4,1): (a) x direction bending strain ξ_x and predicted strain ξ_{pred}; (b) y direction bending strain ξ_y and predicted strain ξ_{pred} (—— dynamic bending strain; —— predicted Strain, ξ_{pred}; – – – propagating wave component of ξ_{pred}; - - - - evanescent wave component of ξ_{pred}).

wave propagation for evanescent waves (via the evanescent bending wavenumbers, $\sqrt{k_x^2 + 2k_y^2}$ and $\sqrt{2k_x^2 + k_y^2}$).

2.3.5. *Farfield correlation of dynamic bending strain and velocity*

Since it is the sum of the dynamic bending strain components which is correlated with velocity (refer equation (14)), the dynamic bending strain components, ξ_x and ξ_y, are always overpredicted in the farfield using velocity predictions based on equation (18) without any allowance for the direction of wave propagation. As the dominant direction of wave propagation varies with frequency and cannot be taken into account using simple velocity measurements, only upper-bound predictions of farfield dynamic bending strain are possible using strain–velocity correlations. This is demonstrated in Figure 2. The predictions are most accurate for the dominant component of dynamic bending strain and at shallow angles of wave propagation.

2.3.6. *Evanescent wave effects*

Evanescent wave effects on dynamic strain and velocity near the clamped boundaries are similar to those observed for the flexural vibration of thin beams [1]. Evanescent waves for the cases considered increase one of dynamic strain and velocity and decrease the other in comparison with the propagating wave component of the response at a particular location (x, y). At the clamped boundaries, for instance, dynamic strain is increased compared with the propagating wave component of the response, whilst velocity is decreased to zero. This prevents the correlation of dynamic strain and velocity at the same position for the prediction of maximum dynamic strain. Evanescent waves also have the effect of increasing the spatial maxima of dynamic strain and velocity above their maximum farfield levels, but by different amounts for fully constrained plates and always at different locations. The factor $K'(f)$ in equation (1) is used to take account of evanescent wave effects on the correlation of dynamic strain and velocity spatial maxima.

2.3.7. *Correlation ratio values*

The non-dimensional correlation ratio $K(f)$ in equations (1) and (2), obtained by combining the factor $K'(f)$ with the non-dimensional shape factor K_{shape}, needs to lie in a small range for practical predictions of maximum dynamic strain in broadband randomly excited plates. $K(f)$ is listed in Table 1 for each of the first 10 natural frequencies of the clamped plate in Figure 1. The values of $K(f)$ are observed to lie in a narrow range (1·7–2·3) supporting the use of equation (2) to obtain conservative narrowband and broadband predictions of maximum dynamic bending strain from measurements of maximum velocity. Also listed in Table 1 are values of the factor $K'(f)$ for the effect of evanescent waves on the farfield correlation ratio. $K'(f)$ is observed to lie in the range 1·0–1·32 for the system under

TABLE 1

Clamped plate natural frequencies, wavenumbers, direction of wave propagation, factor K′ for evanescent wave effects on farfield correlations, and non-dimensional correlation ratio K

	m	n	$f_{m,n}$ (Hz)	k_x	k_y	θ	$K'(f)$	$K(f)$
f_1	1	1	51·5	4·5	7·1	57·6	1·126	1·95
f_2	2	1	83·8	8·6	6·5	37·1	1·103	1·91
f_3	1	2	125·3	4·12	12·5	71·8	1·276	2·21
f_4	3	1	138·1	12·4	6·1	26·2	1·218	2·11
f_5	2	2	154·8	8·15	12·2	56·3	1·137	1·97
f_6	3	2	205·6	12·1	11·8	44·4	1·005	1·74
f_7	4	1	212·4	16·1	5·85	20·0	1·264	2·19
f_8	1	3	236·6	3·97	17·7	77·4	1·322	2·29
f_9	2	3	265·4	7·9	17·5	65·7	1·236	2·14
f_{10}	4	2	277·2	15·8	11·5	36·0	1·114	1·93

consideration. Both $K(f)$ and $K'(f)$ are a function of k_x/k_y being largest when either $k_x \gg k_y$ or $k_y \gg k_x$.

3. CYLINDRICAL SHELL VIBRATION

The correlation of dynamic strain and velocity spatial maxima can also be extended to the vibration of cylindrical shells. As in section 2, farfield relationships between dynamic bending strain and transverse velocity are derived for cylindrical shell vibration using travelling wave solutions. These relationships are found to have a high degree of frequency dependency due to propagating waves that cut-on at higher frequencies, and a resultant velocity parameter based on the spatial maximum of each of the three velocity components is adopted to substantially reduce this frequency dependence. Results for the non-dimensional farfield correlation ratio between the sum of bending strains and the resultant velocity parameter are then compared with values of the non-dimensional correlation ratio between the spatial farfield maxima of the maximum principal strain and resultant velocity calculated for modal vibration of a clamped cylindrical shell. These calculations are used to assess (1) whether the sum of bending strains provides an upperbound for the maximum principal strain, which takes account of both shear strain and bending strain; and (2) whether the farfield relationships derived for individual pairs of propagating waves can be used to provide an upper bound correlation ratio for a combination of propagating waves with different wavenumbers.

Some modal spatial distributions of dynamic bending strain are also presented, indicating the relative significance of axial and circumferential bending strains with circumferential mode number, the location of dynamic strain spatial maxima, and the effects of evanescent waves. Finally, the dynamic strain concentration factor and non-dimensional correlation ratio $K(f)$ are calculated for a clamped cylindrical shell over a range of natural frequencies.

The following analyses are based on the Flugge equations of motion for the free vibration of a thin cylindrical shell ([11, 8]). Only circumferential modes $n = 1$ and above are considered.

3.1. TRAVELLING WAVE SOLUTIONS

Cylindrical shell wave propagation can be expressed in terms of two orthogonal wave components, one in the circumferential direction and the other in the axial direction. Only propagating waves with wavenumber $k_c = n/a$ occur in the circumferential direction resulting in circumferential mode shapes of the form $\cos(n\theta)$, where n is the integral circumferential mode number, θ is the shell angular position and a is the shell mean radius. The circumferential modes are independent of each other and can be analyzed separately. In the axial direction, for a given circumferential mode n, the axial wavenumber is given by $k_a = k_{ns}$ and these waves have the form $\exp(k_{ns}x)$, where x is the axial position along the cylindrical shell axis and s is the particular axial wave.

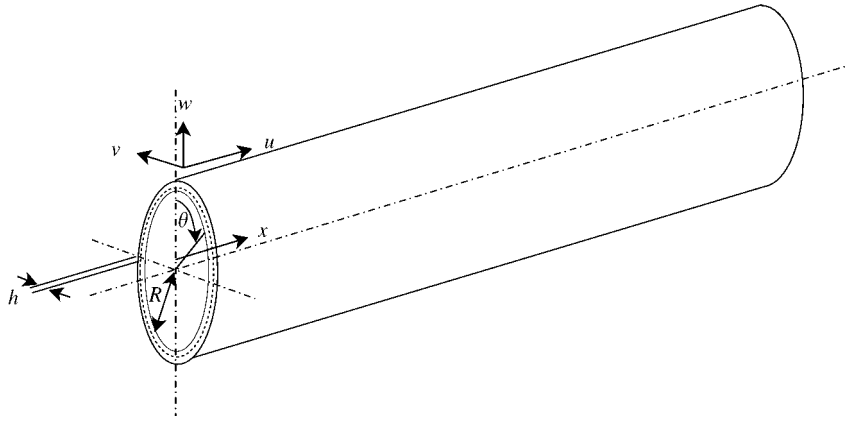

Figure 3. Cylindrical shell coordinate system.

3.1.1. *The travelling wave solution*

Using the separated wave components described above and the co-ordinate system defined in Figure 3, the complete travelling wave solution may be expressed as

$$\boldsymbol{u}(x, \theta, \omega) = \sum_{n=0}^{\infty} \sum_{s=1}^{8} \boldsymbol{U}_{ns} \cos(n\theta) \mathrm{e}^{\boldsymbol{k}_{ns} x}, \tag{19a}$$

$$\boldsymbol{v}(x, \theta, \omega) = \sum_{n=0}^{\infty} \sum_{s=1}^{8} \boldsymbol{V}_{ns} \sin(n\theta) \mathrm{e}^{\boldsymbol{k}_{ns} x} \tag{19b}$$

$$\boldsymbol{w}(x, \theta, \omega) = \sum_{n=0}^{\infty} \sum_{s=1}^{8} \boldsymbol{W}_{ns} \cos(n\theta) \mathrm{e}^{\boldsymbol{k}_{ns} x}, \tag{19c}$$

where $\boldsymbol{u}$, $\boldsymbol{v}$ and $\boldsymbol{w}$ are the complex displacements, $\boldsymbol{U}_{ns}$, $\boldsymbol{V}_{ns}$ and $\boldsymbol{W}_{ns}$ are the complex wave amplitudes for circumferential mode n and axial wave s ($s = 1, \ldots, 8$), and $\omega = 2\pi f$ is the angular frequency.

3.1.2. *Elimination of in-plane wave amplitudes*

Since the out-of-plane radial motions are usually dominant for bending vibration and are the simplest to measure using an accelerometer, the wave amplitude coefficients $\boldsymbol{U}_{ns}$ and $\boldsymbol{V}_{ns}$ for in-plane motion are expressed in terms of the wave amplitude coefficient $\boldsymbol{W}_{ns}$ for out-of-plane motions in order to eliminate these terms and express the travelling wave solution in terms of only out-of-plane displacements. The wave amplitude ratios are defined by $\alpha_{ns} = \boldsymbol{U}_{ns}/\boldsymbol{W}_{ns}$ and $\beta_{ns} = \boldsymbol{V}_{ns}/\boldsymbol{W}_{ns}$ for each root k_{ns} of the characteristic equation. The wave amplitude ratios are obtained by solving the homogeneous matrix equation formed by the equations of motion for $\boldsymbol{U}_{ns}/\boldsymbol{W}_{ns}$ and $\boldsymbol{V}_{ns}/\boldsymbol{W}_{ns}$, and are given by

$$\alpha_{ns} = \frac{\boldsymbol{U}_{ns}}{\boldsymbol{W}_{ns}} = \frac{Q_{12}Q_{23} - Q_{13}Q_{22}}{Q_{11}Q_{22} - Q_{12}Q_{21}} \tag{20}$$

and

$$\beta_{ns} = \frac{\boldsymbol{V}_{ns}}{\boldsymbol{W}_{ns}} = \frac{Q_{13}Q_{21} - Q_{11}Q_{23}}{Q_{11}Q_{22} - Q_{12}Q_{21}}, \tag{21}$$

where the Q_{ij} are defined in Appendix B. The wave amplitude ratios are a function of only the non-dimensional wavenumber $k_{ns}a$, the non-dimensional frequency $\Omega = \omega a/c_L$, the non-dimensional thickness parameter $\beta = h/a\sqrt{12}$, the circumferential mode number n and the Poisson ratio μ. Eliminating $\boldsymbol{U}_{ns}$ and $\boldsymbol{V}_{ns}$ from equation (19) using equations (20) and (21), equation (19) becomes

$$\boldsymbol{u}(x, \theta, \omega) = \sum_{n=0}^{\infty} \sum_{s=1}^{8} \alpha_{ns} \boldsymbol{W}_{ns} \cos(n\theta) \mathrm{e}^{\boldsymbol{k}_{ns} x}, \tag{22a}$$

$$\boldsymbol{v}(x, \theta, \omega) = \sum_{n=0}^{\infty} \sum_{s=1}^{8} \beta_{ns} \boldsymbol{W}_{ns} \sin(n\theta) \mathrm{e}^{\boldsymbol{k}_{ns} x} \tag{22b}$$

and

$$\boldsymbol{w}(x, \theta, \omega) = \sum_{n=0}^{\infty} \sum_{s=1}^{8} \boldsymbol{W}_{ns} \cos(n\theta) \mathrm{e}^{\boldsymbol{k}_{ns} x}. \tag{22c}$$

3.1.3. *Dynamic bending strain*

Dynamic bending strain for circumferential mode n as a function of only the out-of-plane displacements $\boldsymbol{w}$ is obtained by substitution of equation (22) into the strain–displacement equations

$$\xi_x = \frac{\partial u}{\partial x} - z \frac{\partial^2 w}{\partial x^2} \tag{23}$$

and

$$\xi_\theta = \left(\frac{1}{a^2 + az}\right) \left\{ a \frac{\partial v}{\partial \theta} + aw + z \frac{\partial v}{\partial \theta} - z \frac{\partial^2 w}{\partial \theta} \right\} \tag{24}$$

giving

$$\xi_{x,n} = \sum_{s=1}^{8} \boldsymbol{W}_{ns} \mathrm{e}^{\boldsymbol{k}_{ns} x} \cos(n\theta) \{ \boldsymbol{k}_{ns} \alpha_{ns} - z \boldsymbol{k}_{ns}^2 \} \tag{25}$$

and

$$\xi_{\theta,n} = \sum_{s=1}^{8} \boldsymbol{W}_{ns} \mathrm{e}^{\boldsymbol{k}_{ns} x} \cos(n\theta) \left(\frac{1}{a^2 + az}\right) \{ a + n^2 z + na\beta_{ns} + nz\beta_{ns} \}, \tag{26}$$

where ξ_x is the axial component of dynamic bending strain, ξ_θ is the circumferential component of dynamic bending strain, a is the distance from the cylinder axis to the

shell middle surface and z is the distance of a point on the shell wall from the shell middle surface. The maximum and minimum strains occur on the inner and outer surfaces of the shell wall, at $z = \pm h/2$. As the wave amplitude ratios α_{ns} and β_{ns} are calculable at non-dimensional frequency Ω for an arbitrary cylindrical shell with thickness factor β and the Poisson ratio μ, the only unknowns in equations (25) and (26) are the wave amplitude coefficients $\boldsymbol{W}_{ns}$. These coefficients are calculated by evaluating the boundary condition equations for the system under consideration at the natural frequencies Ω_{mn}.

3.1.4. *Velocity*

The velocity response can also be expressed as a function of only $\boldsymbol{W}_{ns}$. Multiplying equation (22) through by $i\omega$ and dropping the summation over n, the velocity response for circumferential mode n is given by

$$\dot{\boldsymbol{u}}_n(x, \theta, \omega) = i\omega \sum_{s=1}^{8} \alpha_{ns} \boldsymbol{W}_{ns} \cos(n\theta)\, e^{\boldsymbol{k}_{ns} x}, \tag{27a}$$

$$\dot{\boldsymbol{v}}_n(x, \theta, \omega) = i\omega \sum_{s=1}^{8} \beta_{ns} \boldsymbol{W}_{ns} \sin(n\theta)\, e^{\boldsymbol{k}_{ns} x} \tag{27b}$$

and

$$\dot{\boldsymbol{w}}_n(x, \theta, \omega) = i\omega \sum_{s=1}^{8} \boldsymbol{W}_{ns} \cos(n\theta)\, e^{\boldsymbol{k}_{ns} x}. \tag{27c}$$

It should be noted that equations (25)–(27) above are for a particular circumferential mode n only. The complete response is the superposition of the response due to each of the excited circumferential modes.

3.2. FARFIELD RELATIONSHIPS

Generalizing the farfield relationship in equation (15) between dynamic strain and velocity for the possible case of K_{shape} being frequency dependent,

$$K_{shape}(f) = \frac{[\xi_{x,FF}(x, y, f) + \xi_{y,FF}(x, y, f)]\, c_L}{v_{FF}(x, y, f)} \equiv K_{FF}(f), \tag{28}$$

where K_{FF} is defined as the non-dimensional farfield correlation ratio. The aim of this section is to derive relationships for K_{FF} and investigate its dependence on frequency. Only axial and circumferential dynamic bending strains are considered initially since the shear strain is zero at angular positions where the axial and circumferential dynamic bending strains are largest (shear strain is a function of $\sin(n\theta)$, whereas the bending strain components are both a function of $\cos(n\theta)$). At the end of this section, farfield correlations between maximum principal strain

(which combines the bending and shear strains into a single equivalent uniaxial value of dynamic strain) and velocity for a clamped cylindrical shell system are compared with farfield correlation ratios calculated using the formulas derived in this subsection. Results presented in the figures are limited to the $n = 1$ and 3 circumferential modes.

3.2.1. *Relationships for axial and circumferential dynamic strain based on transverse velocity*

The farfield relationship between axial dynamic strain and transverse velocity for propagating waves with wavenumber k_{ns} is obtained by substituting equations (25) and (27c) into equation (28) and dropping the summation over s, yielding

$$K_{FF,axial,ns,\dot{w}}(f) = \frac{|\xi_{x,ns} c_L|}{|\dot{\boldsymbol{w}}_{ns}|} = \left| \frac{\boldsymbol{k}_{ns}\boldsymbol{\alpha}_{ns} - z\boldsymbol{k}_{ns}^2}{\mathrm{i}\omega} \right| c_L, \tag{29}$$

where $\xi_{x,ns}$ is the axial dynamic strain for a propagating wave with wavenumber $\boldsymbol{k}_{ns}$, $\dot{\boldsymbol{w}}_{ns}$ is the transverse velocity for the same propagating wave, and both the wave amplitude ratios $\boldsymbol{W}_{ns}$ and dependence on circumferential position θ have cancelled out. The above relationship was derived for a single propagating wave but also applies to the superposition of two propagating waves travelling in opposite directions with equal wavenumbers. Substitution of $k_{n,s+1} = -k_{ns}$ to give a propagating wave in the opposite direction has no effect on equation (29) (since $\alpha_{n,s+1} = -\alpha_{n,s}$ from equation (20), $k_{n,s+1}\alpha_{n,s+1} = k_{n,s}\alpha_{n,s}$ and $zk_{n,s+1}^2 = zk_{n,s}^2$). Which does not apply to the superposition of propagating waves with unequal wavenumbers.

Similarly, for circumferential dynamic strain the non-dimensional farfield correlation ratio is given by

$$K_{FF,circ,ns,\dot{w}}(f) = \frac{|\xi_{\theta,ns} c_L|}{|\dot{\boldsymbol{w}}_{ns}|} = \left(\frac{1}{a^2 + az} \right) \left| \frac{\{a + n^2 z + na\beta_{ns} + nz\beta_{ns}\}}{\mathrm{i}\omega} \right| c_L, \tag{30}$$

where $\xi_{\theta,ns}$ is the circumferential dynamic strain for a propagating wave with wavenumber k_{ns}, and $\dot{\boldsymbol{w}}_{ns}$ is the transverse velocity for the same propagating wave. This relationship also holds for two propagating waves travelling in opposite directions with the same wavenumber (equation (30) is unchanged for $k_{n,s+1} = -k_{n,s}$ as $\beta_{n,s+1} = \beta_{ns}$ from equation (21)), but does not hold for a combination of propagating waves with unequal wavenumbers.

The non-dimensional farfield correlation ratios for axial and circumferential dynamic strains, calculated from equations (29) and (30) at $z = h/2$ for circumferential modes $n = 1$ and 3, are plotted in Figure 4 for the $k1$, $k2$ and $k3$ propagating wave pairs of a cylindrical shell system with thickness factor $\beta = 0{\cdot}0192$. The $k1$ waves are defined as the propagating waves with the lowest cut-on frequency for a given circumferential mode, whilst the $k2$ and $k3$ waves are the propagating waves with higher cut-on frequencies. The $k1$ wave correlation ratios in Figure 4 are bounded by the non-dimensional correlation ratio for plate flexural vibration,

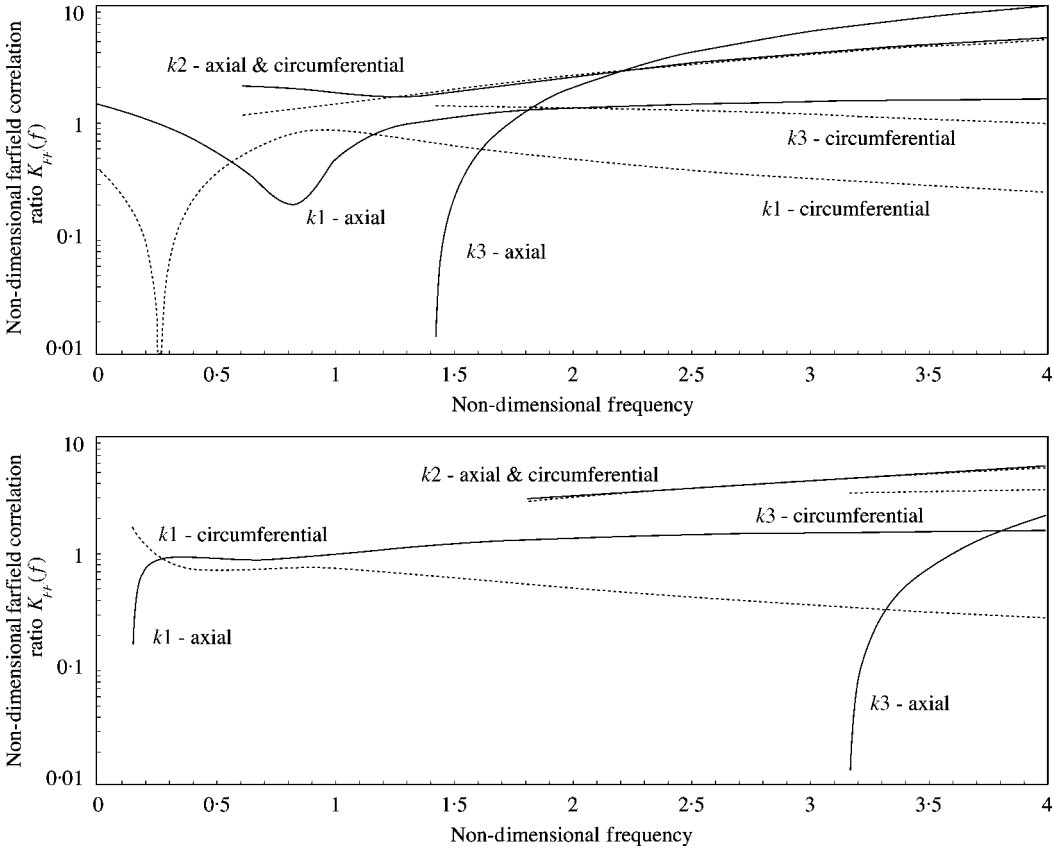

Figure 4. Non-dimensional farfield correlation ratio between dynamic bending strain and transverse velocity ($\beta = 0{\cdot}0192$): (a) $n = 1$; (b) $n = 3$ (—— axial strain; - - - - circumferential strain).

$K_{shape} = \sqrt{3}$. The $k2$ and $k3$ waves however have correlation ratios that increase significantly above K_{shape} at higher frequencies. Alternative definitions of equations (29) and (30) are needed to decrease this frequency dependence.

3.2.2. *Farfield relationships based on resultant velocity*

Larger values of K_{FF} for the $k2$ and $k3$ wave pairs result from large in-plane and small out-of-plane motions relative to dynamic strain. To account for these effects, dynamic strain is correlated with the resultant velocity of all three velocity components in place of the transverse velocity. It is also necessary to use spatial maximum farfield values of dynamic strain and the three velocity components rather than their values at the same position to account for their different spatial distributions (the correlation of bending strain and transverse velocity is a special case where correlation at the same position is possible). The farfield relationship between dynamic strain and velocity for circumferential mode n and axial wave s is then

$$K_{FF,\varepsilon,ns}(f) = \frac{|\xi_{\varepsilon,FF,max,ns}(f)c_L|}{\sqrt{|\dot{\boldsymbol{u}}_{FF,max,ns}(f)|^2 + |\dot{\boldsymbol{v}}_{FF,max,ns}(f)|^2 + |\dot{\boldsymbol{w}}_{FF,max,ns}(f)|^2}}, \tag{31}$$

where the subscript "*max*" denotes the spatial maximum value over the surface of the cylindrical shell, and ε represents either axial strain ($\xi_\varepsilon = \xi_x$), circumferential strain ($\xi_\varepsilon = \xi_\theta$) or the sum of bending strains ($\xi_\varepsilon = \xi_x + \xi_\theta$).

Expansion of equation (31) reveals that $K_{FF,\varepsilon,ns}$ can be expressed in terms of non-dimensional farfield correlation ratios between ξ_ε and the individual velocity components,

$$K_{FF,\varepsilon,ns,\dot{u}}(f) = \frac{|\xi_{\varepsilon,FF,max,ns}(f)\, c_L|}{|\dot{\boldsymbol{u}}_{FF,max,ns}(f)|}, \tag{32a}$$

$$K_{FF,\varepsilon,ns,\dot{v}}(f) = \frac{|\xi_{\varepsilon,FF,max,ns}(f)\, c_L|}{|\dot{\boldsymbol{v}}_{FF,max,ns}(f)|} \tag{32b}$$

and

$$K_{FF,\varepsilon,ns,\dot{w}}(f) = \frac{|\xi_{\varepsilon,FF,max,ns}(f)\, c_L|}{|\dot{\boldsymbol{w}}_{FF,max,ns}(f)|}, \tag{32c}$$

using the relation

$$\frac{1}{K^2_{FF,\varepsilon,ns}} = \frac{1}{K^2_{FF,\varepsilon,ns,\dot{u}}} + \frac{1}{K^2_{FF,\varepsilon,ns,\dot{v}}} + \frac{1}{K^2_{FF,\varepsilon,ns,\dot{w}}}. \tag{33}$$

$K_{FF,\varepsilon,ns,\dot{w}}$ is evaluated using equation (29) and/or equation (30) depending on the strain of interest (ξ_x, ξ_θ or $\xi_x + \xi_\theta$). Equations for $K_{FF,\varepsilon,ns,\dot{u}}$ and $K_{FF,\varepsilon,ns,\dot{v}}$ are obtained by redefining the wave amplitude ratios in equations (25)–(27) in terms of $\mathbf{U}_{ns}$ and $\mathbf{V}_{ns}$ respectively, and then deriving similar expressions to equations (29) and (30). It should be noted that the terms $\sin(n\theta)$ and $\cos(n\theta)$ in equation (27) both equal unity for spatial maximum values of the velocity components about the circumference.

$K_{FF,\varepsilon,ns}$ from equation (31) is plotted in Figure 5 for the axial and circumferential dynamic strains for each pair of propagating waves $k1$, $k2$ and $k3$. The curves are bounded by $K_{shape} = \sqrt{3}$ (the shape factor for plate flexural vibration) for both circumferential modes considered and for all three pairs of propagating waves.

3.2.3. *Farfield correlations for sum of bending strains and principal strain*

The non-dimensional correlation ratio $K_{FF,princ,n}$ for the farfield principal strain ($\xi_\varepsilon = \xi_{princ}$), which takes account of both bending and shear strain, is plotted in Figure 6 over a range of natural frequencies for modal vibration of the cylindrical shell system in Figure 7. The non-dimensional correlation ratio presented in this case is for all propagating waves acting simultaneously. Also shown in Figure 6 is $K_{FF,\varepsilon,ns}$ for the sum of bending strains $\xi_\varepsilon = \xi_x + \xi_\theta$. $K_{FF,princ,n}$ was evaluated using equation (31) and calculated spatial maximum farfield values of principal strain and velocity for modal vibration of the cylindrical shell system in Figure 7. "Farfield" values of dynamic strain and velocity were obtained for each mode by identifying the wave type of each wave $s = 1, \ldots, 8$, and only including propagating waves in the

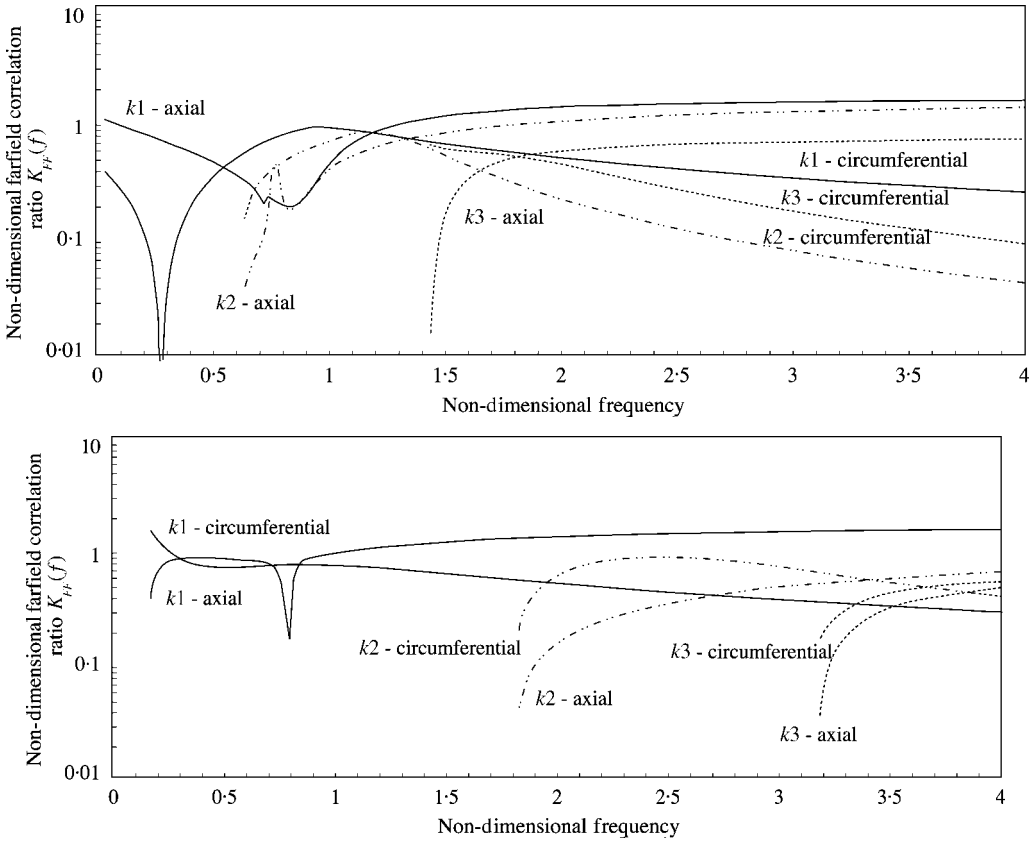

Figure 5. Non-dimensional farfield correlation ratio between dynamic bending strain and resultant velocity ($\beta = 0{\cdot}0192$): (a) $n = 1$; (b) $n = 3$ (—— $k1$;—- - -— $k2$; - - - $k3$).

summation over axial wave number s in equations (25)–(27). $K_{FF,\varepsilon,ns}$ for the sum of bending strains $\xi_\varepsilon = \xi_x + \xi_\theta$ was evaluated using equation (33). This latter calculation is system independent and only requires that the non-dimensional thickness parameter be known, but is limited to only one pair of propagating waves acting at a time.

The non-dimensional farfield correlation ratio $K_{FF,princ,n}$ for principal strain lies in a small range and is similar in magnitude between circumferential modes supporting the selection of a frequency-independent farfield correlation ratio (step changes in the correlation ratio between modes are due to variations in the relative dominance of the velocity and strain components with axial and circumferential mode number). Furthermore, the largest non-dimensional farfield correlation ratio $K_{FF,\varepsilon,ns}$ for the sum of bending strains is seen to provide an upper-bound curve for $K_{FF,princ,n}$. This indicates that the sum of bending strains can be correlated with the resultant velocity parameter defined in equation (31) to provide an upper-bound curve for the farfield correlation ratio between principal dynamic strain and resultant velocity, taking account of both bending and shear strains for all three pairs of propagating waves acting simultaneously.

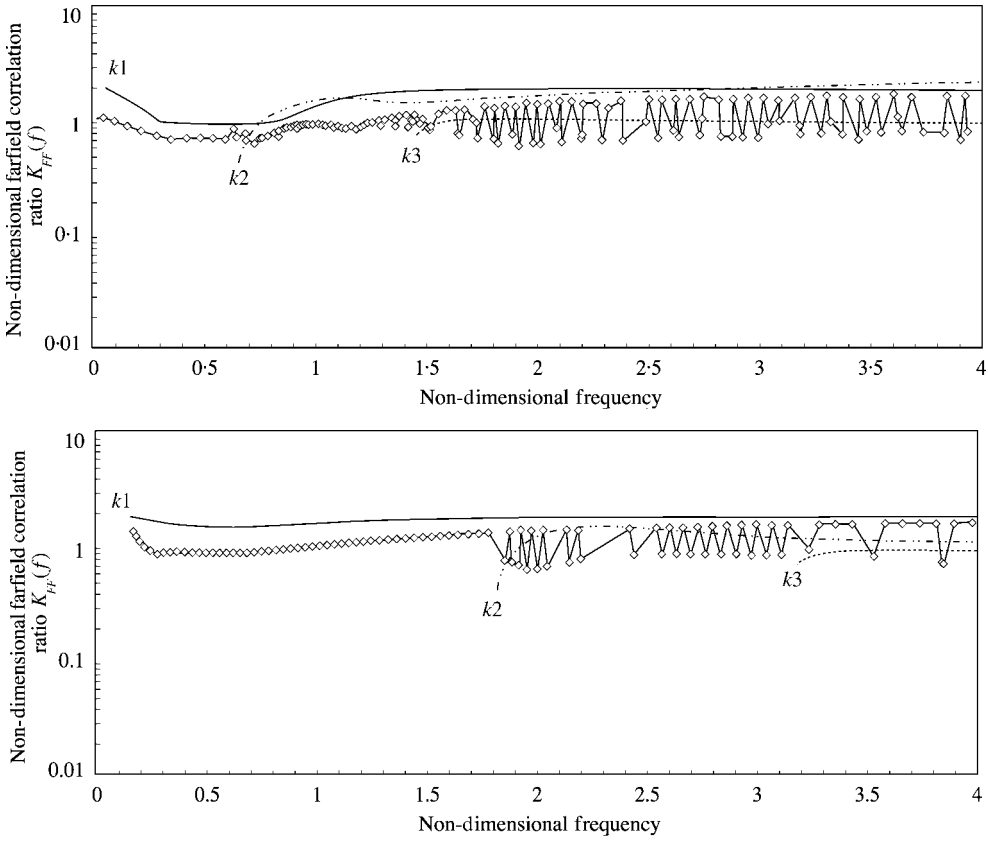

Figure 6. Non-dimensional farfield correlation ratio between the sum of bending strains and resultant velocity. Also shown is the non-dimensional farfield correlation ratio between the spatial maximum farfield principal strain and resultant velocity (—— $k1$; — - - — $k2$; - - - $k3$; ◇ principal strain correlation ratio).

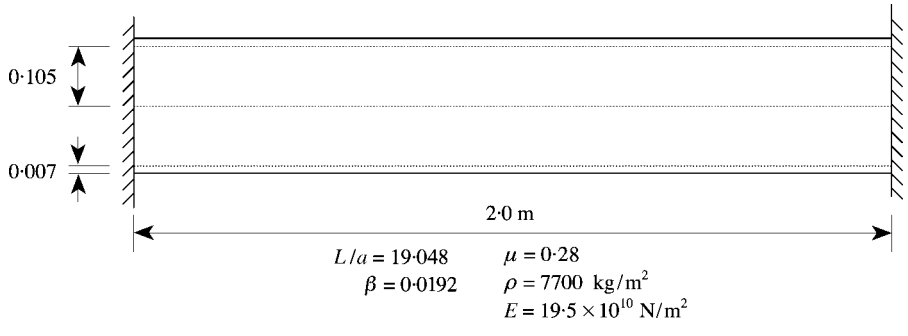

Figure 7. Clamped cylindrical shell system.

3.3. DYNAMIC STRAIN AND VELOCITY MODAL SPATIAL DISTRIBUTIONS

Modal spatial distributions of axial dynamic strain, circumferential dynamic strain and transverse velocity are plotted in Figure 8 for the clamped cylindrical

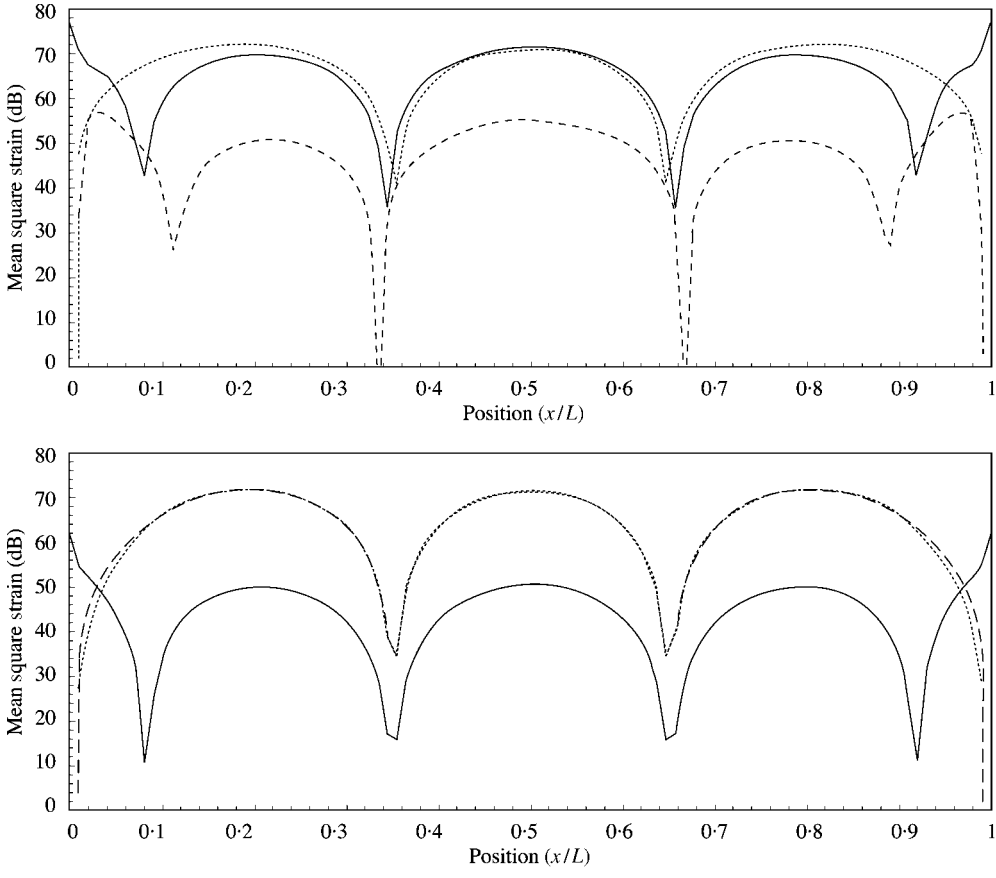

Figure 8. Modal spatial distributions of dynamic strain for the clamped cylindrical shell: (a) mode (3, 1); (b) mode (3, 3) (—— axial bending strain ξ_x; – – – circumferential bending strain, ξ_θ; ------ predicted strain ξ_{pred}).

shell system in Figure 7. These spatial distributions are plotted for the third axial mode of circumferential modes $n = 1$ and 3. The third axial mode is used since both nearfield and farfield conditions exist for this mode. Dimensions and material properties for the clamped cylindrical shell system are given in Figure 7, and the system ring frequency is 7946 Hz. These calculations were performed using the procedures described in Karczub [10].

Only dynamic strain on the outer surface of the shell wall at $\theta = 0$ is considered here. The angular position $\theta = 0$ is the circumferential position of maximum axial and circumferential dynamic bending strain, and the dynamic shear strain at this angular position is equal to zero.

3.3.1 *Axial and circumferential dynamic bending strain*

The axial and circumferential dynamic strains for the clamped cylindrical shell vary in relative significance with circumferential mode number as shown by the results in Figure 8 for axial mode $m = 3$. For circumferential mode $n = 1$ (Figure 8(a)) the axial strain is significantly larger than the circumferential strain; for $n = 2$

the axial and circumferential strains are approximately equal (not shown); and for $n = 3$ (Figure 8(b)) the circumferential strain is significantly larger than the axial strain. The increasing relative significance of circumferential dynamic strain with circumferential mode number is associated with the increasing value of the circumferential wavenumber k_c relative to the axial wavenumber k_a. This is the same effect as observed for thin plate vibration, and is associated with the changing direction of wave propagation as the wavenumber or mode number in one direction is varied.

3.3.2. *Locations of maximum dynamic bending strain*

The locations of maximum dynamic strain are different for axial and circumferential dynamic bending strain. Maximum axial bending strain occurs at the clamped boundaries, whereas maximum circumferential bending strain occurs away from the clamped boundaries at a position which varies with axial mode number. Since the angular position of maximum strain will also vary between modes depending on the location of excitation and whether axial or circumferential strain is dominant, the selection of suitable locations to install strain gauges for the measurement of maximum dynamic bending strain is quite difficult.

Consideration also needs to be given to whether maximum dynamic strain occurs on the inner or outer surface of the cylindrical shell. For the first and third circumferential modes considered here, axial strain is largest on the external wall surface ($z = -h/2$), whilst the circumferential strain is the same on the inner and outer walls for $n = 1$ and largest on the internal wall surface for $n = 3$. At much higher frequencies the opposite may be true depending on: (1) the relative values of the farfield correlation ratio at $z = \pm h/2$; and (2) the effects of evanescent waves in nearfield regions.

3.3.3. *Farfield relationships between dynamic bending strain and velocity*

In Figure 8, the transverse velocity component has been scaled by the farfield correlation ratio for the dominant component of dynamic bending strain (the axial component for $n = 1$, and the circumferential component for $n = 3$). The resulting prediction of dynamic strain accurately predicts the maximum dynamic strain in farfield regions. The farfield correlation ratios used in Figure 8 were calculated for $k1$ waves only, since only the $k1$ waves are propagating waves at the frequencies of interest.

3.3.4. *Evanescent wave effects*

The spatial distributions of axial and circumferential dynamic strain in Figure 8 are clearly influenced by evanescent waves. Evanescent wave effects increase axial dynamic strain at the clamped boundaries, and increase circumferential dynamic strain in regions near the clamped boundaries.

The propagating and evanescent wave components of axial dynamic strain associated with the $k1$, $k2$, $k3$ and $k4$ waves are plotted separately in Figure 9 for mode (3, 1). The $k1$ waves are propagating waves; the $k2$ waves are Type 2 evanescent waves (purely decaying) with the same wavelength as the propagating waves; and the $k3$ and $k4$ waves are Type 3 and Type 4 evanescent waves (propagating

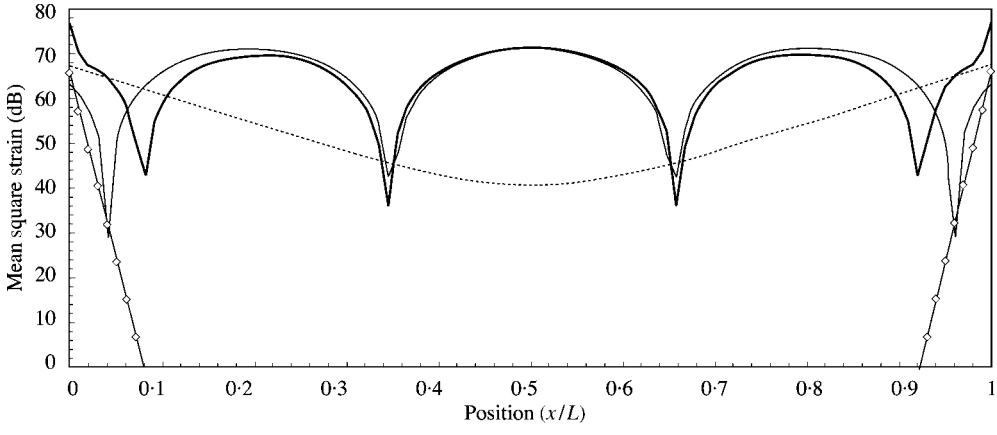

Figure 9 Modal spatial distributions of axial dynamic strain for mode (3, 1) of the clamped cylindrical shell. (——— total dynamic strain; —— $k1$ propagating wave component of dynamic strain; ------ $k2$ evanescent wave component; —◇— $k3$ and $k4$ evanescent wave components).

decaying waves) which have much shorter wavelengths (refer Karczub [10]). The spatial distributions for the $k1$ and $k2$ waves are very similar to the spatial distributions for the respective propagating and evanescent wave components of a clamped beam. The $k3$ and $k4$ waves are additional evanescent waves that cause a sharp increase in axial dynamic strain at the clamped boundaries. At frequencies where the axial dynamic strain is dominant, evanescent waves also cause a significant increase in circumferential dynamic strain close to the clamped boundaries (refer Figure 8).

Due to the additional evanescent waves present in a cylindrical shell at low frequencies, dynamic strain concentration effects may be larger in cylindrical shells than in beams. It should be noted that a very fine mesh is required in finite element calculations in order to correctly model the dynamic strains associated with the short-wavelength evanescent wave components of the response.

3.4. DYNAMIC STRAIN CONCENTRATION FACTORS

The dynamic strain concentration factor is defined as the ratio of the spatial maximum dynamic strain to the spatial maximum dynamic strain associated with propagating waves in the absence of evanescent waves. Figure 10 gives the dynamic strain concentration factor at the natural frequencies of the clamped cylindrical shell system for circumferential modes $n = 1$ and 3. The maximum value of the dynamic strain concentration factor is 2.1 for $n = 1$ and 2·2 for $n = 3$. For comparison, the maximum dynamic strain concentration factor for a clamped beam is 1.42. Dynamic strain concentration is larger for clamped cylindrical shells than for clamped beams due mainly to the additional evanescent waves of short wavelength at low frequencies. At higher frequencies where there is only one pair of evanescent waves, the maximum dynamic strain concentration for cylindrical shell vibration is only slightly larger than 1·42 (1·6 for $n = 1$ and 1·46 for $n = 3$)

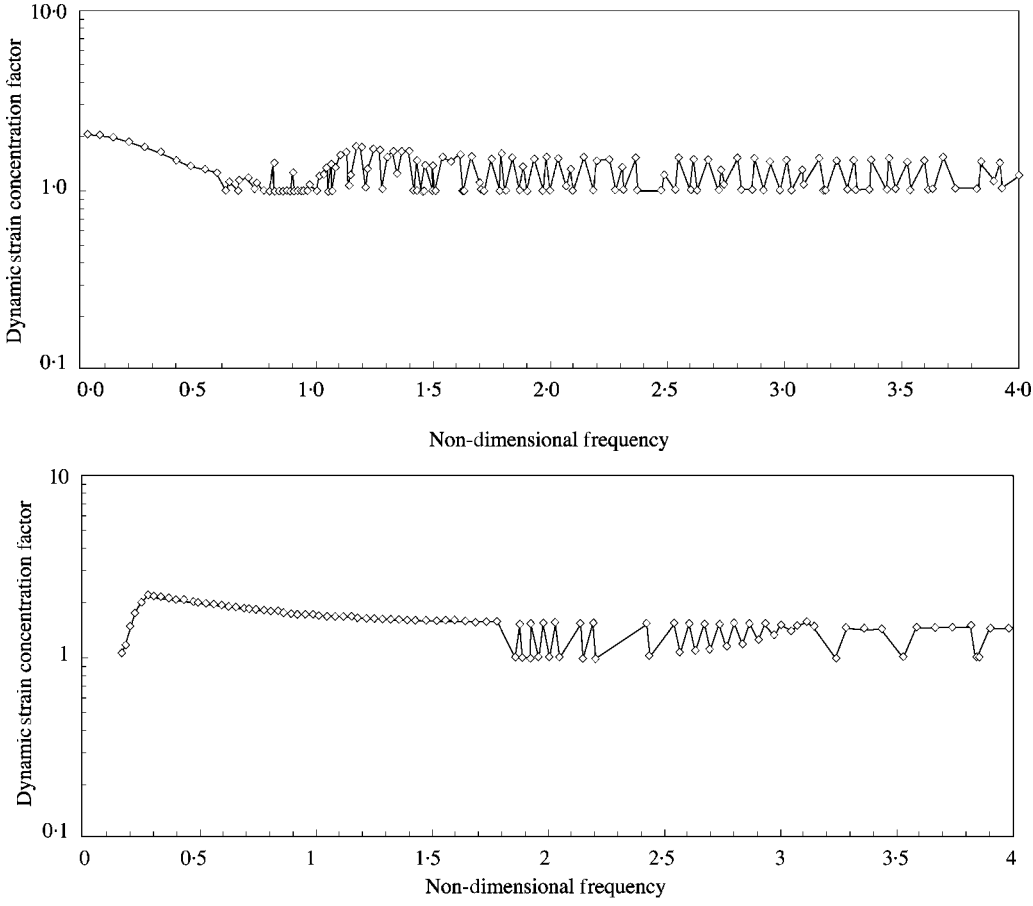

Figure 10. Dynamic strain concentration factor for modal vibration of a clamped cylindrical shell based on the maximum principal strain: (a) $n = 1$; (b) $n = 3$.

3.5. CORRELATION OF DYNAMIC STRAIN AND VELOCITY SPATIAL MAXIMA

Modal correlation ratios $K(f_n)$ between the spatial maxima of principal dynamic strain and resultant velocity (calculated from the spatial maximum of each velocity component) are plotted in Figure 11. The correlation ratio lies in a range of 0·8–2·6 with an average of 1·5 for circumferential mode $n = 1$, and lies in a range of 0.7–2·3 with an average of 1·7 for mode $n = 3$. The spatial maxima used to calculate $K(f_n)$ are the spatial maxima over the whole surface of the cylindrical shell system. The results in Figure 11 support the selection of an upper-bound frequency-independent correlation ratio for conservative broadband predictions of maximum overall dynamic strain.

4. EXPERIMENTS

4.1. CLAMPED RECTANGULAR PLATE

A clamped rectangular plate was tested experimentally to obtain data demonstrating dynamic strain and velocity spatial distributions, and the

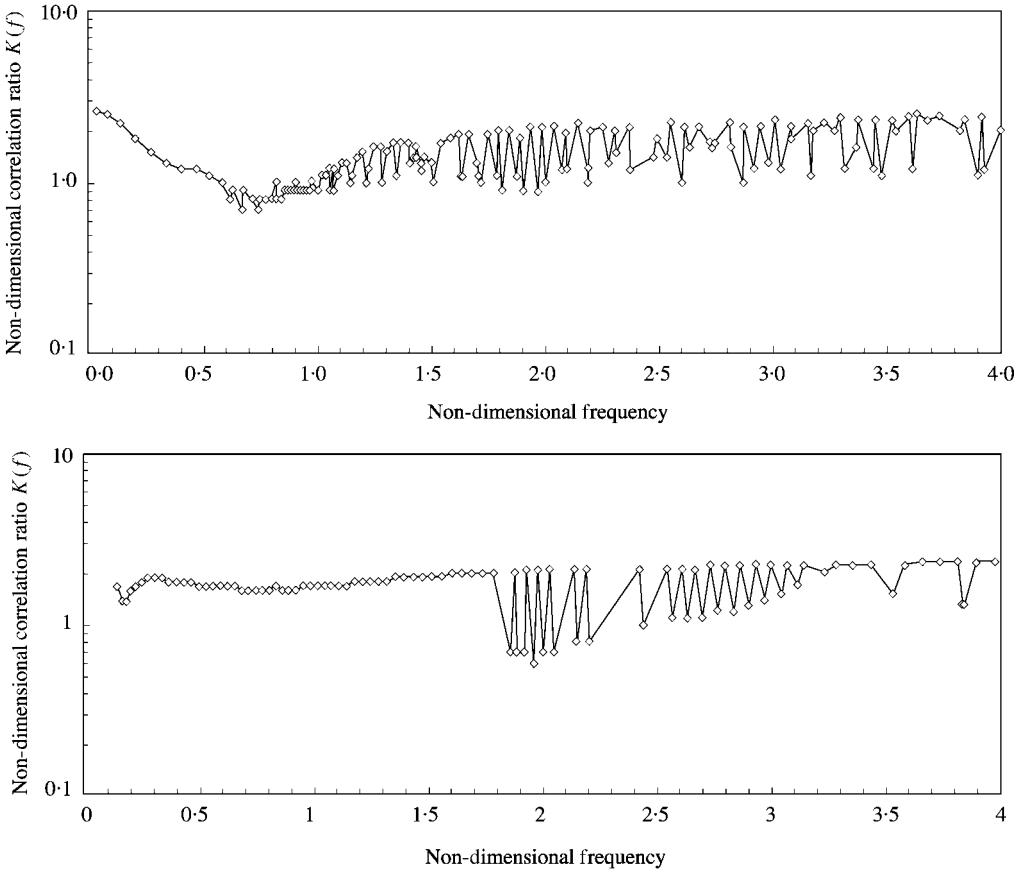

Figure 11. Non-dimensional correlation ratio for modal vibration of a clamped cylindrical shell based on the maximum principal strain and the resultant velocity: (a) $n = 1$; (b) $n = 3$.

correlation of dynamic strain and velocity spatial maxima as a function of frequency. These results show that whilst dynamic strain is dependent upon the direction of wave propagation, narrowband estimates of maximum dynamic strain from velocity are possible based on the farfield relationship in equation (15). The clamped rectangular plate used in the experiments is shown in Figure 12. The plate was clamped on all sides and excited by a point force at the position shown. Strain gauges were located on the plate surface along a line normal to one of the clamped boundaries, 0·2 m from the nearest parallel boundary. The strain gauge positions are given in Table 2. The first five calculated and measured resonant frequencies of the clamped plate system are listed in Table 3.

4.1.1. *Spatial distributions*

Measured and predicted dynamic strain spatial distributions in the x direction are presented in Figure 13(a) for a resonant frequency with the wavenumber component magnitude in the x direction larger than in the y direction ($k_x > k_y$). Spatial distributions in the x direction for a mode with wavenumber component

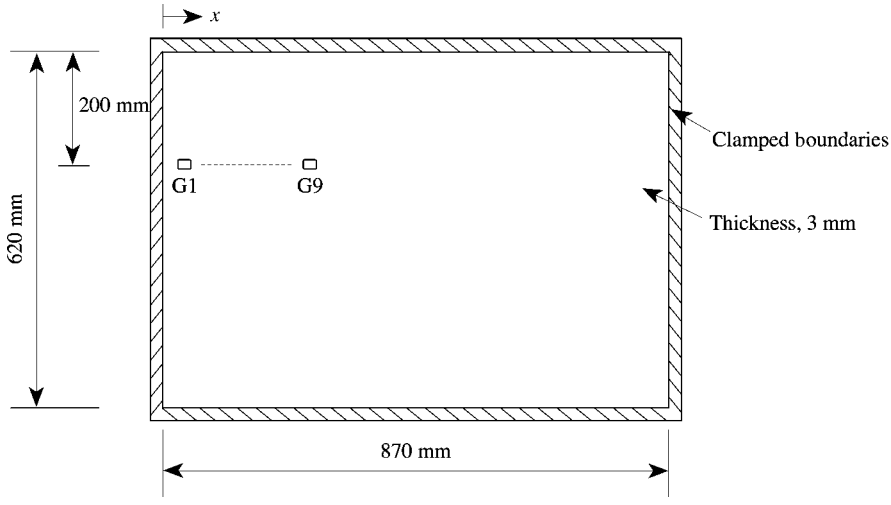

Figure 12. Clamped plate experimental arrangement.

TABLE 2

Strain gauge labels and positions for the clamped plate

Strain gauge	Position (m)
1	0·002
2	0·025
3	0·045
4	0·085
5	0·125
6	0·165
7	0·205
8	0·24
9	0·285

TABLE 3

Calculated and measured natural frequencies of the clamped plate system

Mode	m	n	Calculated $f_{m,n}$ (Hz)	Measured $f_{m,n}$ (Hz)
1	1	1	52	41
2	2	1	84	77
3	1	2	125	115
4	3	1	138	130
5	2	2	155	145

magnitudes in the y direction larger than in the x direction ($k_y > k_x$) are presented in Figure 13(b). The predicted dynamic strain in each case was obtained by scaling the measured velocity by the farfield correlation ratio for dynamic strain using the relationship in equation (15).

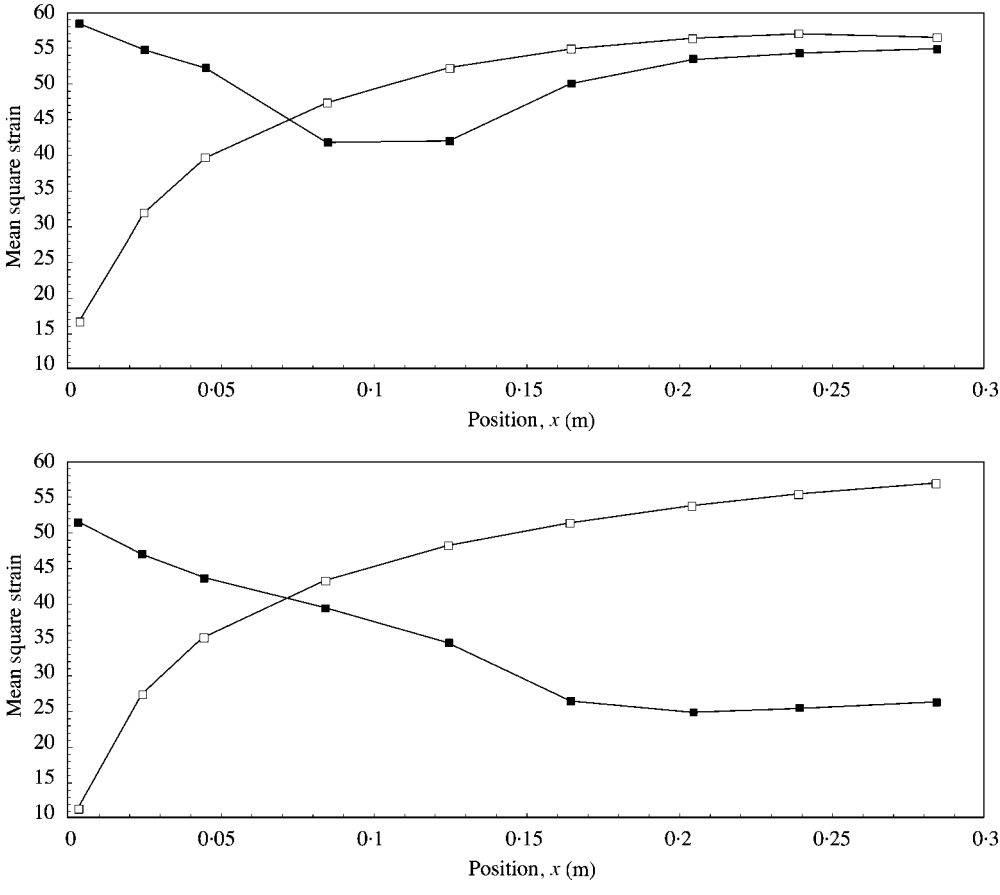

Figure 13. Measured and predicted dynamic strain spatial distributions for a fully clamped plate along the line $y = 0{\cdot}2$ m: (a) $k_x > k_y$; (b) $k_y > k_x$ (—■— measured; —□— predicted).

Maximum measured dynamic strain occurs at the clamped boundary in each case due to dynamic strain concentration. For the case of $k_x > k_y$ (Figure 13(a)), the maximum measured strain is larger than the maximum predicted dynamic strain, whereas for $k_y > k_x$ (Figure 13(b)) the maximum predicted dynamic strain is largest. At locations away from the plate boundaries, for the case of $k_x > k_y$, the measured strain is only slightly less than the predicted dynamic strain, whereas for $k_y > k_x$ the measured strain is significantly less that the predicted dynamic strain. These effects are due to the dependence of the propagating wave components of dynamic bending strain on the direction of wave propagation (refer equations (9) and (10)).

4.1.2. *Autospectral prediction of maximum dynamic strain*

Maximum dynamic strain along the line where strain gauges were installed occurs at the clamped boundary. The measured dynamic strain at this location is compared in Figure 14 with a velocity prediction of the maximum dynamic strain along this line obtained using (1) the maximum measured velocity in each frequency band along the line where strain gauges were installed, and (2) the farfield

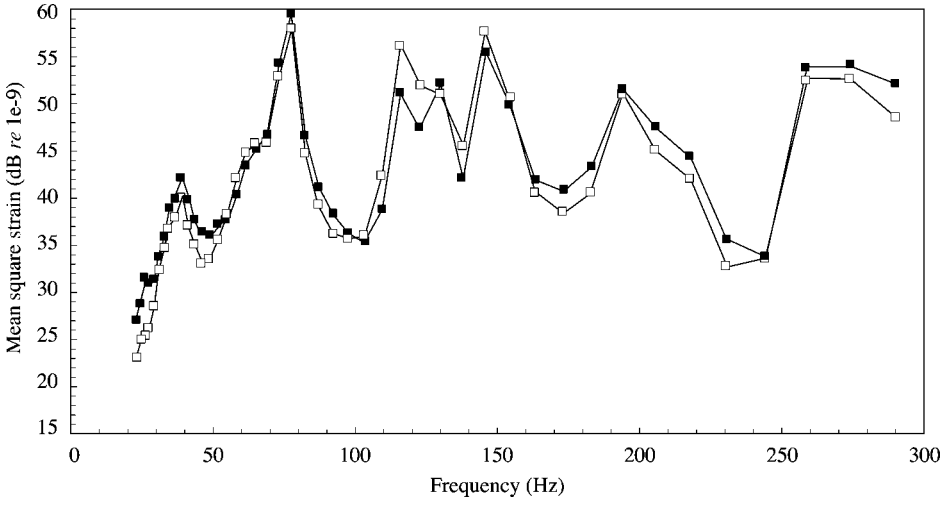

Figure 14. Measured and predicted dynamic strain autospectra at the clamped boundary of a fully clamped plate for the line $y = 0{\cdot}2$ m (—■— measured; —□— predicted).

correlation ratio for dynamic strain. No allowance has been made for dynamic strain concentration. Dynamic strain at the boundary in the direction parallel to the clamped boundary can be neglected as it decreases to zero at the clamped boundary since the velocity decreases to zero (refer to equations (6) and (7); dynamic bending strain is proportional to the one-dimensional mode shape in the normal direction). The predicted dynamic strain underpredicts and overpredicts depending on the particular mode and the direction of wave propagation, but otherwise the agreement between measured and predicted is quite good. By including a factor for dynamic strain concentration, conservative predictions of overall dynamic strain should be possible. Hence, by extending the velocity measurements to the whole structure, conservative predictions of maximum overall dynamic strain appear feasible.

4.2. CYLINDRICAL SHELL FARFIELD RELATIONSHIPS

Measurements of dynamic strain and velocity at the same position on the outer surface of a cylindrical shell were performed to obtain data demonstrating farfield correlations between (1) circumferential dynamic strain and transverse velocity; (2) axial dynamic strain and transverse velocity; and (3) the sum of the dynamic bending strain components and transverse velocity. A free–free cylindrical shell with an annular ring half-way along its length was used as the test structure (Figure 15). The cylindrical shell is 3 m long, has a mean radius of 0·105 m and is 0·007 m thick. Free–free boundaries were simulated by using steel cables to support the structure at each end. Strain gauges were attached in the axial and circumferential directions at $x = 0{\cdot}75$ m. The strain gauges were positioned at the top of the cylindrical shell and the exciting force was applied at the bottom of the cylindrical shell at $x = 0{\cdot}5$ m, as shown in Figure 15.

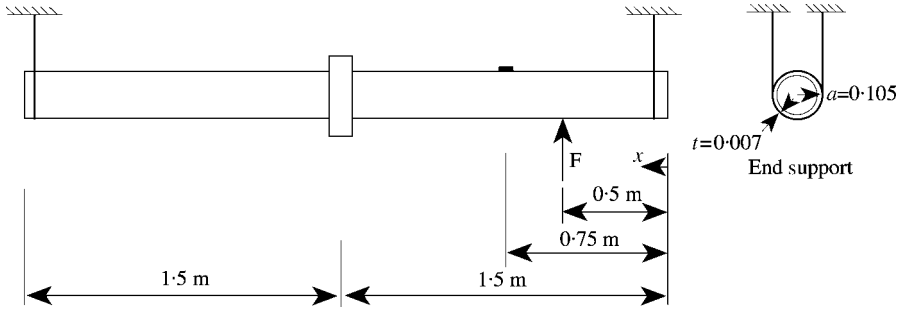

Figure 15. Cylindrical shell experimental arrangement.

4.2.1. *Farfield predictions—axial and circumferential dynamic strain*

The farfield velocity prediction of dynamic strain at $x = 0{\cdot}75$ m is compared with the measured axial dynamic strain in Figure 16(a), and with the measured circumferential dynamic strain in Figure 16(b). The predicted dynamic strain was calculated from the measured transverse velocity using a non-dimensional farfield correlation ratio of $\sqrt{3}$. There is good agreement between predicted dynamic strain and measured circumferential dynamic strain at most frequencies, with the predictions being conservative at most frequencies. Frequencies at which circumferential dynamic strain is significantly overestimated correspond to frequencies at which the axial dynamic strain is dominant; axial dynamic strain is itself accurately predicted at these frequencies, whilst being overpredicted at those frequencies where the circumferential dynamic strain is dominant. The relative correlations of axial and circumferential dynamic strain vary with frequency due to variations in the relative magnitudes of axial and circumferential dynamic strain associated with changes in the direction of wave propagation. The lack of correlation at anti-resonant frequencies is due to the noise floor of the strain measurements.

4.2.2. *Farfield predictions—sum of bending strains*

The sum of the measured components of dynamic bending strain is compared with the predicted dynamic strain in Figure 17. The correlation between measured and predicted is quite good in this case. Variations between measured and predicted are due to (1) variations in the farfield correlation ratio with frequency and between the $k1$, $k2$ and $k3$ waves (refer Figure 4); (2) possibly some nearfield effects for modes with small axial mode number; and (3) the 22 dB noise floor of the strain measurements which affects predictions at antiresonant frequencies and at frequencies below the first resonant frequency (below 350 Hz).

5. SUMMARY AND CONCLUSIONS

Correlations between dynamic strain and velocity were investigated for the flexural vibration of clamped rectangular plates and the vibration of clamped cylindrical shell systems. The results show that the correlation ratio between dynamic strain and velocity for these systems lies in a small range. This supports

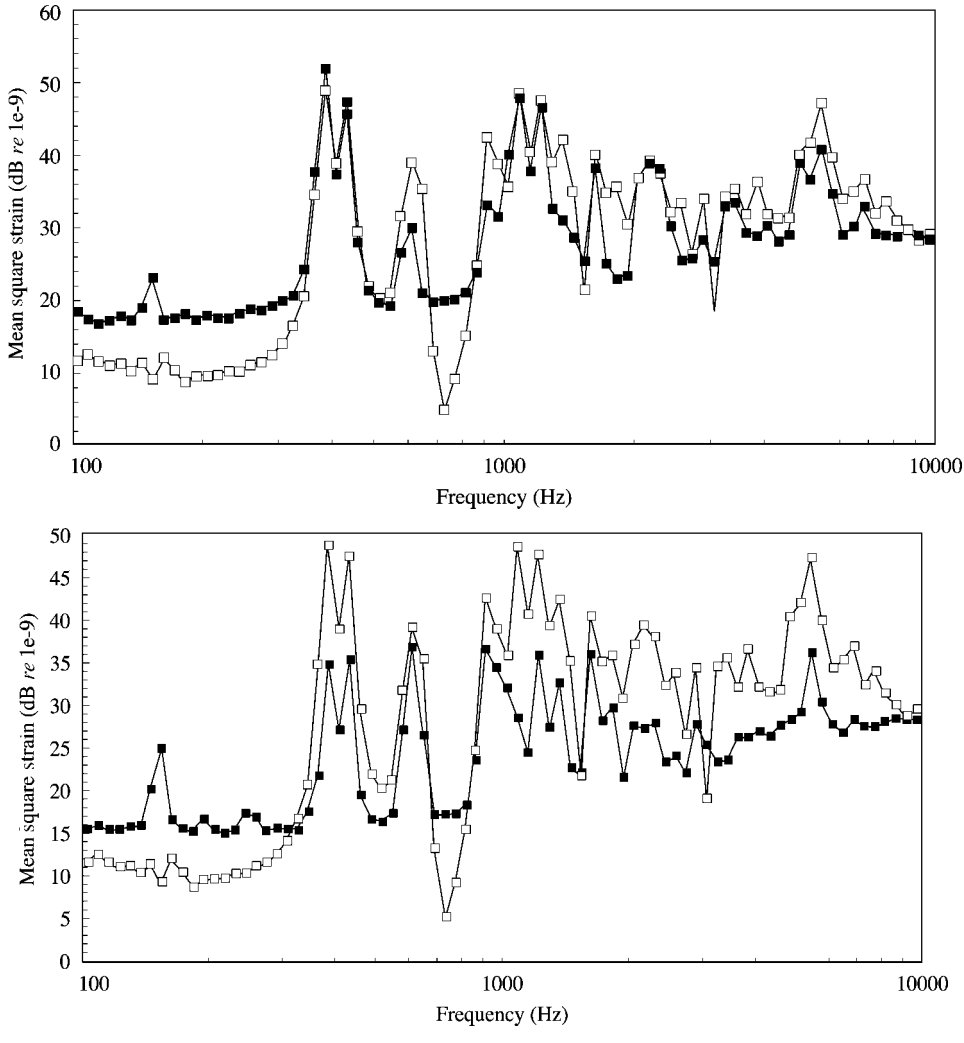

Figure 16. Measured and predicted dynamic strain autospectra at $x = 0{\cdot}75$ m of the cylindrical shell experimental rig. (—■— measured; —□— predicted): (a) axial dynamic strain; (b) circumferential dynamic strain.

the use of equations (1) and (2) with upper-bound frequency-independent non-dimensional correlation ratios for broadband conservative predictions of spatial maximum dynamic strain in constrained rectangular plate and cylindrical shell systems. In the case of cylindrical shell vibration, the resultant of the spatial maximum of each of the three velocity components should be correlated with dynamic strain rather than the transverse velocity to minimize the complicating effects of waves with large in-plane and small out-of-plane motions. The derived farfield relationships are also largely frequency independent and are independent of boundary conditions providing the basis for generalization of these results to plate and cylindrical shell systems with other boundary conditions.

The results also demonstrate that spatial maximum levels of dynamic strain occur in the nearfield region of systems with clamped boundaries due to the

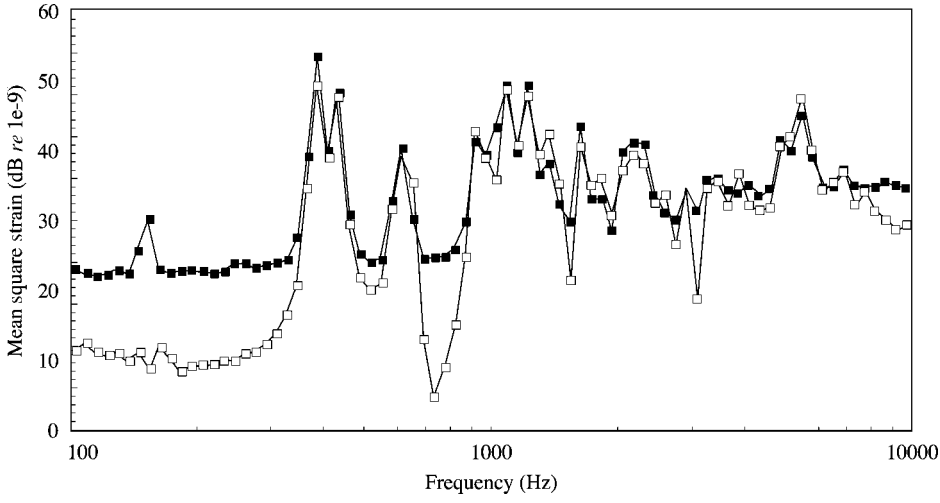

Figure 17 Sum of axial and circumferential (—■— sum of measured axial and circumferential strain; —□— predicted strain).

influence of evanescent waves. The increase in spatial maximum dynamic strain over spatial maximum farfield levels is defined as dynamic strain concentration. The level of dynamic strain concentration is significant and must be taken into account when analyzing the fatigue life of structures. An important consideration for finite element modelling and measurements of maximum dynamic strain is the short spatial extent of high dynamic strain. The spatial extent of high dynamic strain (levels at or close to the spatial maximum level) at clamped boundaries is small and decreases as the wavenumber of evanescent waves increases. In the case of cylindrical shell vibration, there are additional pairs of evanescent waves in the low- to mid-frequency range with much shorter wavelength that result in even larger levels of dynamic strain concentration over an even smaller spatial extent. Due to these effects of evanescent waves, (1) a very fine mesh is required for finite element calculations in order to correctly model dynamic strains at clamped boundaries; and (2) very short length strain gauges located right at the clamped boundary are required to measure maximum levels of dynamic strain.

REFERENCES

1. D. G. Karczub and M. P. Norton 1998 *Journal of Sound and Vibration* **226**(4), 645–674. Correlations between dynamic stress and velocity in randomly excited beams.
2. F. V. Hunt 1960 *The Journal of the Acoustical Society of America* **32**, 1123–1128. Stress and strain limits on the attainable velocity in mechanical vibration.
3. E. E. Ungar 1962 *Journal of Engineering for Industry* **84**, 149–155. Maximum Stresses in beams and plates vibrating at resonance.
4. S. M. Stearn 1970 *Ph.D. Thesis, Southampton University*. Stress distributions in randomly excited structures
5. S. M. Stearn 1971 *Journal of Sound and Vibration* **15**, 353–365. The concentration of dynamic stress in a plate at a sharp change of section.

6. M. P. Norton and F. J. Fahy 1988 *Noise Control Engineering Journal* **30**, 107–117. Experiments on the correlation of dynamic stress and strain with pipe wall vibrations for statistical energy analysis applications.
7. E. E. Ungar 1961 *The Journal of the Acoustical Society of America* **33**, 633–639. Transmission of plate flexural waves through reinforcing beams; dynamic stress concentrations.
8. K. Forsberg 1964 *AIAA Journal* **2**, 2150–2157. Influence of boundary conditions on the modal characteristics of thin cylindrical shells.
9. C. R. Steele 1963 *Lockheed Missiles and Space Co., TR* 6-90-63-84. Shells with edge loads of rapid variation.
10. D. G. Karczub 1996 *Ph.D. Thesis, The University of Western Australia*. The prediction of dynamic stress and strain in randomly vibrating structures using vibrational velocity measurements.
11. A. W. Leissa, 1973 *NASA SP*-288. Vibration of Shells.
12. R. B. Bhat, J. Singh and G. Mundkur 1993 *Journal of Vibration and Acoustics* **115**, 177–181. Plate characteristic functions and natural frequencies of vibration of plates by iterative reduction of partial differential equation.

APPENDIX A

Natural frequencies obtained using the approximate travelling wave solution for clamped plate flexural vibration are compared with published values in Table 4. The published values of natural frequency are taken from Bhat *et al.* [12]. The non-dimensional frequency Ω used in Table 4 is related to the frequency f,

TABLE 4

Comparison of approximate travelling wave solution calculations of non-dimensional natural frequency with published data from Bhat [12] *for a clamped rectangular plate with a length-to-width ratio of* 2

		Approximate Solution			Bhat [12]
m	n	$k_x a$	$k_y a$	$\Omega_{m,n}$	$\Omega_{m,n}$
1	1	1·84	4·58	97·5	98·3
2	1	3·61	4·29	125·8	127·3
3	1	5·31	4·02	177·6	179·1
4	1	6·95	3·84	252·2	253·4
2	2	3·43	7·69	283·5	284·3
2	3	3·35	10·9	521·0	521·4
2	4	3·30	14·8	837·2	837·5
3	2	5·12	7·53	331·8	331·1
3	3	5·01	10·82	568·7	569·5
3	4	4·95	14·03	884·9	885·5
4	2	6·78	7·38	401·7	403·2
4	3	6·67	10·71	636·8	637·9
4	4	6·59	13·95	952·5	953·4

wavenumber components k_x and k_y, and wavenumber k by

$$\Omega = 2\pi f a^2 \sqrt{\frac{\rho_s}{D}} = (k_x a)^2 + (k_y a)^2 = k^2 a^2, \tag{A.1}$$

where f is frequency, ρ_s is mass per unit length, D is bending stiffness, a is plate thickness, and k_x and k_y are the x- and y-components of bending wavenumber k.

APPENDIX B

The matrix elements of the matrix $[Q_{ij}]$ are given by:

$$Q_{11} = -n^2\mu_1 - \beta^2 n^2 \mu_1 + \Omega^2 + (k_{ns}a)^2,$$

$$Q_{12} = n\mu_3 k_{ns} a,$$

$$Q_{13} = \mu k_{ns} a - \beta^2 n^2 \mu_1 k_{ns} a - \beta^2 (k_{ns}a)^3,$$

$$Q_{21} = -n\mu_3 k_{ns} a,$$

$$Q_{22} = -n^2 + \Omega^2 + \mu_1 (k_{ns}a)^2 + 3\beta^2 \mu_1 (k_{ns}a)^2,$$

$$Q_{23} = -n + \beta^2 n \mu_4 (k_{ns}a)^2,$$

$$Q_{31} = \mu k_{ns} a - \beta^2 n^2 \mu_1 k_{ns} a - \beta^2 (k_{ns}a)^3,$$

$$Q_{32} = n - \beta^2 n \mu_4 (k_{ns}a)^2,$$

$$Q_{33} = 1 + \beta^2 - 2\beta^2 n^2 + \beta^2 n^4 - \Omega^2 - 2\beta^2 n^2 (k_{ns}a)^2 + \beta^2 (k_{ns}a)^4.$$

The constants μ_1, μ_2, μ_3 and μ_4 have been used to simplify the above equations and are defined by

$$\mu_1 = \frac{1-\mu}{2},$$

$$\mu_2 = 1 - \mu^2,$$

$$\mu_3 = \frac{1+\mu}{2},$$

and

$$\mu_4 = \frac{3-\mu}{2},$$

The non-dimensional frequency Ω for cylindrical shell vibration is defined as

$$\Omega = \omega a \sqrt{\frac{\rho(1-\mu^2)}{E}} = \frac{\omega a}{c_L},$$

where a is the shell mean radius and c_L is the longitudinal wavespeed for a thin plate.